Research Square

Preprints are preliminary reports that have not undergone peer review.
They should not be considered conclusive, used to inform clinical practice,
or referenced by the media as validated information.

Automated Classification and Quantification of Fungal Spores in Aerobiological Sampling Using Deep Learning

Dámaris A. Jiménez-Uribe

duribe@utb.edu.co

School of Engineering, Architecture and Design, Universidad Tecnologica de Bolivar, Cartagena de Indias, Colombia
https://orcid.org/0000-0002-3084-1340

Deyson Gómez Sánchez

School of Engineering, Architecture and Design, Universidad Tecnologica de Bolivar, Cartagena de Indias, Colombia

Jeison D. Jimenez

School of Engineering, Architecture and Design, Universidad Tecnologica de Bolivar, Cartagena de Indias, Colombia

Rosa Acevedo-Barrios

Department of Basic Sciences, Universidad Tecnologica de Bolivar, Cartagena de Indias, Colombia

Carolina Rubiano-Labrador

Department of Basic Sciences, Universidad Tecnologica de Bolivar, Cartagena de Indias, Colombia

Hernando Altamar-Mercado

Department of Basic Sciences, Universidad Tecnologica de Bolivar, Cartagena de Indias, Colombia

Alberto Patiño-Vanegas

Department of Basic Sciences, Universidad Tecnologica de Bolivar, Cartagena de Indias, Colombia

Research Article

Keywords: aerobiological sampling, atmospheric allergens, bioaerosols, convolutional neural networks, deep learning, environmental monitoring, fungal spores, object detection

Posted Date: July 7th, 2026

DOI: https://doi.org/10.21203/rs.3.rs-9997567/v1

License: This work is licensed under a Creative Commons Attribution 4.0 International License. Read Full License

Abstract

Airborne fungal spores are important bioaerosols because of their relevance to environmental monitoring and respiratory health. However, routine aerobiological assessment still relies on manual microscopic counting, a time-consuming procedure prone to inter-observer variability and delayed data availability. Here, we developed and validated a deep learning-based approach for the automatic detection and quantification of eight fungal genera in microscopic images obtained by Hirst-type volumetric sampling in Santa Marta, Colombia. Three detection strategies were compared: YOLO26, ViT-B/16 + Faster R-CNN, and AlexNet + Faster R-CNN. After dataset re-splitting and offline/online augmentation to reduce class imbalance and improve generalization, YOLO26l achieved the best performance (*recall* = 0.812, *precision* = 0.823, mAP@0.5 = 0.846, F1-score = 0.817). In an external set of 516 unseen images, it maintained a *precision* of 0.803 and a *recall* of 0.659. Automated and manual counts were positively and significantly correlated for all genera (Spearman's ρ = 0.387–0.852; p < 0.001). The model processed 516 images in 1 min 39 s, compared with 2.8 h required for manual counting. These results highlight the potential of deep learning to strengthen and scale routine aerobiological monitoring for environmental bioaerosol surveillance and public health applications.

1. Introducción

Up to 25% of atmospheric pollution may consist of bioaerosols, airborne particles produced by living organisms, including pollen, seeds, bacteria, fungi, algae, protozoa, and waste products (Cao et al. 2014). Among these, fungal spores constitute a representative and environmentally relevant bioaerosol group because, owing to their small size and efficient wind-mediated dispersal, they exhibit high atmospheric mobility and can remain present in the air throughout the year (Pashley et al. 2012; Egan et al. 2014). Exposure to fungal spores has been associated with several health conditions, including asthma, chronic obstructive pulmonary disease (COPD), irritation, and allergic rhinitis, with pediatric and adolescent populations being particularly affected (Nieguitsila et al. 2007; Spicer and Gangloff 2010; Lee et al. 2016; Humbal et al. 2018). These allergic diseases have shown a yearly increase, which has been linked to rising atmospheric concentrations of fungal spores associated with air pollution and climate change (Lundbäck et al. 2016). In addition to their health effects, allergic diseases impose a substantial economic burden through direct medical expenses, productivity losses, and reduced quality of life among affected individuals (Charalampopoulos et al. 2022).

The prediction of allergic disease incidence associated with fungal spores requires identifying the fungal genera present in the atmosphere and characterizing relevant physical attributes, including particle size, concentration, and infectious capacity (Twaroch et al. 2016). These variables are determined through aerobiological monitoring using volumetric samplers, which are designed to capture suspended airborne particles and promote their adhesion onto a sampling surface for subsequent optical microscopy analysis (Blais-Lecours et al. 2015; Lee et al. 2016). However, a recent systematic review indicates that during the last 15 years, aerobiological monitoring has been conducted in only approximately 30 countries, whereas in regions such as the Americas, Africa, and Oceania, these programs remain scarce or absent (Jiménez-Uribe et al. 2026). One of the main constraints limiting broader monitoring coverage is that fungal spore classification and counting remain meticulous and time-consuming tasks that require specialized personnel, while the final results are still influenced by the uncertainty associated with the observer's expertise (Adamov et al. 2024; Tummon et al. 2024).

In recent years, methodologies aimed at automating this process have consequently been developed. An early line of work consisted of applying classical computer vision to microscopy images: the particle was first isolated through segmentation, and handcrafted shape and texture descriptors were then extracted and finally classified using traditional methods such as k-NN or SVM (Marcos et al. 2015). Related strategies have also been applied to fungal spores, combining image processing with color, texture, and shape descriptors together with conventional classifiers (Soltani Nezhad et al. 2024). However, these approaches often rely on stable segmentation and on parameters tuned to specific illumination, focus, and artifact conditions; therefore, their performance may deteriorate when particle overlap occurs (Battiato et al. 2020). In addition, because they are based on feature engineering, they require the manual selection of discriminative traits, a process that depends on the researcher's expertise and is less robust when subtle morphological variability exists among taxa (Zolfaghari and Sajedi 2024).

Within this context, convolutional neural networks (CNNs) have gained increasing relevance because they can automatically learn discriminative patterns directly from the image, thereby facilitating the efficient identification and classification of objects

of interest (Gheorghe et al. 2024; Sapkota et al. 2025). The implementation of neural networks for automated pollen analysis has achieved recognition rates of up to 96% (Li and Flenley 1999; France et al. 2000; Tello-Mijares and Flores 2016). More recently, the availability of images from diverse pollen types has improved the training of convolutional networks; in particular, datasets such as POLLEN13K and POLLEN73S have been developed and used with models including AlexNet, SmallerVGGNet, DenseNet-201, and ResNet-50, achieving accuracies ranging from 85% to 95.7% (Battiato et al. 2020; Astolfi et al. 2020).

CNNs were originally developed mainly for object classification. However, in automatic detection tasks relevant to aerobiological monitoring, object classification alone is insufficient, as spatial localization is also required. To address this, the object detection algorithm “You Only Look Once” (YOLO) was introduced in 2015. YOLO performs detection and classification within a single neural network, thereby substantially reducing computational time. This deep learning algorithm divides the image into a grid and directly predicts bounding boxes and class probabilities for each cell (Bi et al. 2025).

YOLO has been applied in different scientific fields for the detection and classification of objects in microscopic images. In biological applications, it has been used for cell identification (Waithe et al. 2020), stomatal detection in leaves of different plant species (Casado-García et al. 2020), pollen grain recognition (Cao et al. 2020), and the identification of diseases caused by fungi (Tahir et al. 2018; Nair et al. 2021).

Despite advances in automated pollen recognition, the classification of fungal spores has progressed more slowly, partly because their sampling and annotation are more challenging than those of pollen grains. To date, many automated systems have been developed under single-genus conditions, for example for *Alternaria* spp., and have focused on total counts obtained from automatic bioaerosol monitors (González-Alonso et al. 2023). This emphasis on monogeneric scenarios limits the applicability of automated systems in atmospheres characterized by greater taxonomic diversity and highlights the need for multigenus methods and databases capable of representing the real variability of airborne fungal spores and enabling the simultaneous identification of multiple genera (Bruffaerts et al. 2025).

To address this limitation, the present study develops a deep learning-based system for the detection and automatic counting of fungal spores belonging to eight genera in microscopic images. The proposed workflow includes image acquisition through volumetric aerobiological sampling, manual spore annotation, and the construction of an in-house database for training detection models. Three models with different architectures were trained, and the best-performing model was selected according to its performance. Practical applicability was then evaluated using previously unseen images, and the results were compared with those obtained by traditional manual counting. Overall, this study broadens the taxonomic scope of automation in environmental aerobiology and provides a reference framework for the development of more scalable and efficient systems, with the potential to reduce the workload associated with microscopic analysis and to support the timely generation of information for environmental surveillance and public health risk assessment.

2. Methods

The aim of this study was to perform the automatic counting of fungal spores from microscopic images using deep learning models. The workflow implemented for model development in this study is shown in Fig. 1. First, the construction and preprocessing of the dataset are described; second, the evaluated architectures are presented; and finally, the training settings and evaluation metrics, the comparative analysis framework across architectures, and the statistical validation of the results are detailed.

2.1. Dataset

2.1.1. Dataset original

The images were obtained from the aerobiological sampling campaign conducted between June 1, 2023, and May 31, 2024, in Santa Marta, Colombia, using a Hirst-type volumetric sampler. Sample processing was carried out in strict accordance with the protocol established by the Spanish Aerobiology Network (Galán et al. 2007). From the total number of processed images, 325 were randomly selected. These images were acquired using an Olympus CX43 microscope at 400× magnification and an

Olympus EP50 camera, which generated images of 2592 × 1944 pixels. To facilitate annotation, each image was subdivided into four equal quadrants of 1296 × 972 pixels (Crespo-Michel et al. 2023).

The dataset annotation process was performed using Roboflow (Dwyer et al. 2026), an online platform specialized in the management and annotation of computer vision datasets. For each image, bounding boxes were applied to identify and classify each spore according to its fungal genus. Eight classes/genera were defined based on their high abundance in the sampling campaign and their relevance as potential allergens reported in the literature (Fig. 2): *Cladosporium, Coprinus, Curvularia, Didymella, Ganoderma, Leptosphaeria, Nigrospora*, and *Xylaria* (Grinn-Gofroń and Bosiacka 2015; Levetin et al. 2016; Pomés et al. 2016; Nair et al. 2021). The annotations were stored in YOLO format, which records, for each instance, the class (genus) together with the normalized coordinates of the bounding box center, as well as its width and height.

The original dataset comprised 1281 images and 2252 labels (instances), distributed across the training, validation, and test subsets (Table 1.). The class/genus-level analysis revealed two main limitations. First, the dataset showed genus imbalance, with *Coprinus* as the most represented genus (20.1%) and *Nigrospora* as the least represented (9.1%). Second, the allocation of images to the training subset was heterogeneous across genera, with values ranging from 62.2% for *Coprinus* to 90.2% for *Nigrospora*. These differences could affect the representativeness of the validation and test subsets and, consequently, the robustness of model evaluation.

Table 1
Distribution of images and labels across subsets in the original dataset.

Subset	Images	Labels
Train	920	1 581
Validation	257	485
Test	104	186

2.1.2. Dataset modifications

To address the limitations identified in the original dataset, three main modifications were implemented. First, a new stratified split of the images was performed into 70% for training, 20% for validation, and 10% for testing, using the predominant spore type in each image as the reference criterion. The validation and test subsets were composed exclusively of original images, without data augmentation, to ensure an unbiased evaluation of model performance.

Second, offline data augmentation was applied to the training subset to reduce genus imbalance. A target of 320 instances per class was established, taking as reference the most represented class after the new split (*Coprinus*, 316 instances), and synthetic samples were generated for the less represented genera using the Albumentations library (Buslaev et al. 2020). The transformations included geometric operations, photometric adjustments, and image degradation simulations to improve model robustness to variations in orientation, size, illumination, and focus. Bounding boxes were adjusted according to each transformation, and those with visibility below 40% were discarded.

Finally, online data augmentation was enabled during YOLOv26 training, that is, transformations automatically applied during the loading of each mini batch. This included mosaic (probability = 1.0), which is useful for increasing object density per image in a dataset with a low average number of instances (1.79 objects/image), and mixup (probability = 0.1) as a regularization mechanism. More specifically, mosaic combines several images into a single image, thereby increasing the number of visible spores per image, whereas mixup blends two images in a controlled manner to generate intermediate examples. This strategy helps reduce overfitting and improve the generalization capacity of the model (Zhang et al. 2018; Bochkovskiy et al. 2020).

2.1.3. Resulting dataset

The final dataset comprised 1574 images with 2963 instances in the training set, 264 images with 512 instances in the validation set, and 131 images with 290 instances in the test set. Table 2 summarizes the evolution of the class distribution

during dataset preparation, including the original training distribution, the stratified re-split, and the final training set after offline augmentation. The largest relative increases were observed for initially underrepresented genera, including Cladosporium, Nigrospora, Curvularia, and Leptosphaeria. This strategy reduced the imbalance in the training set and potentially decreased the risk of model bias toward the most represented generation. Because augmentation was applied at the image level rather than at the individual-instance level, the final number of training instances per genus could exceed the target value of 320 when augmented images contained multiple annotated objects.

Table 2
Class distribution across dataset preparation stages.

Genus	Original training set	Re-split training set	Validation set	Test set	Final augmented training set	Increase after augmentation
Cladosporium	219	78	147	70	239	206%
Coprinus	281	316	86	50	446	41%
Curvularia	175	149	45	24	346	132%
Didymosphaeria	206	212	56	36	394	86%
Ganoderma	176	195	52	29	346	77%
Leptosphaeria	158	163	37	29	371	128%
Nigrospora	184	143	40	21	343	140%
Xylaria	182	194	49	31	378	95%
Total	**1581**	**1250**	**512**	**290**	**2963**	—

2.2. Models structure

In this study, three automatic object detection approaches were compared to identify and classify airborne fungal spores in microscopic images: the YOLO family, a hybrid detector based on a Vision Transformer coupled with Faster R-CNN, and a deep convolutional network based on AlexNet. All models were adapted to recognize eight fungal genera: *Cladosporium, Coprinus, Curvularia, Didymella, Ganoderma, Leptosphaeria, Nigrospora*, and *Xylaria*. These architectures were selected because they enable the evaluation of different image analysis strategies for scenes containing multiple small objects within the same field of view, while maintaining a balance between recognition capability and computational efficiency (Battiato et al. 2020; Zhao et al. 2024).

2.2.1. YOLO26

YOLO26 is an object detection architecture designed to identify and classify elements directly within an image in a single process (Hidayatullah and Tubagus 2026). In this study, two variants were evaluated: Medium (YOLO26m) and Large (YOLO26l), which share the same general structure but differ in processing capacity. The base architecture is shown in Fig. 3. As input, architecture received images of 1280 × 1280 pixels, a higher resolution than that commonly used, to better preserve the morphological details of the spores. In general terms, the YOLO26 architecture enables the extraction of visual information from the image, the integration of features at different scales, and, ultimately, the localization and classification of the objects present. This strategy is well suited to microscopic images, where several small spores may appear within the same field of view. In the present study, the original architecture was adapted exclusively to recognize the eight fungal genera included in the analysis.

2.2.2. ViT + Faster R-CNN

As a second architecture, a hybrid detector combining two components was evaluated: a Vision Transformer (ViT-B/16), responsible for “reading” the image and extracting relevant visual patterns, and Faster R-CNN, which uses this information to propose potential spore locations and subsequently classify them by genus (Ren et al. 2017; Dosovitskiy et al. 2021). In this implementation, a single representation scale was used: the model extracted one set of image features and based on it,

performed spore detection and classification (Fig. 4). To reduce overfitting, the first six layers of the ViT were kept frozen during training so that they retained the general patterns learned previously, while only the layers closer to the specific task were fine-tuned. Using the extracted features, Faster R-CNN generated candidate regions and assigned one of the eight fungal genera to each detection. Finally, a filtering step was applied to retain only the highest-confidence predictions, thereby reducing unreliable detections.

2.2.3. AlexNet + Faster R-CNN

As a third architecture, a modified version of AlexNet with batch normalization, coupled with a Faster R-CNN detector, was evaluated (Ren et al. 2017; Krizhevsky et al. 2017). The model received images resized to 640 × 640 pixels and generated a single feature map, from which the detector proposed regions of interest and performed the classification of the eight fungal genera analyzed (Fig. 5). Final detections were filtered to retain only the most reliable predictions. Training was performed for a maximum of 100 epochs, with progressive adjustment of the learning rate and early stopping to reduce the risk of overfitting.

2.3. Training configuration and evaluation metrics

The four architectures were trained using the same augmented dataset described in Section 2.1, although the input resolution, optimizer, and learning-rate adjustment scheme were defined according to each architecture. The main hyperparameters are summarized in Table 3.

Table 3
Training hyperparameters for each evaluated architecture.

Parameter	YOLO26m	YOLO26l	ViT-B/16 + Faster R-CNN	AlexNet + Faster R-CNN
Input resolution (px)	1 280	1 280	1 280	640
Maximum epochs	150	150	100	100
Patience (early stopping)	30	30	20	30
Batch size	8	8	4	16
Learning rate	0.01	0.01	0.0001	0.01
Weight decay	0.0005	0.0005	0.05	0.0005
Momentum	0.937	0.937	—	0.9
Optimizer	MuSGD (auto)	MuSGD (auto)	AdamW + CosineAnnealingLR	SGD + CosineAnnealingLR
Trainable parameters	~ 25 M	~ 43 M	57.9 M	18.3 M
Confidence threshold	0.25	0.25	0.25	0.25
IoU threshold (NMS)	0.45	0.45	0.45	0.45

The YOLO26m and YOLO26l variants shared the same training configuration and differed only in architecture size, which allowed the effect of representational capacity on performance to be evaluated. For the YOLO variants and ViT-B/16 + Faster R-CNN, an input resolution of 1280 pixels was used to preserve, as much as possible, the detail of the original subimages (1296 × 972 pixels). In contrast, AlexNet + Faster R-CNN was trained with images of 640 pixels, consistent with its lower representational capacity, and was optimized using stochastic gradient descent with a momentum of 0.9. With 18.3 million trainable parameters, it was the most compact architecture evaluated in the study.

2.4. Evaluation metrics

Model performance was evaluated using *precision*, *recall*, and mean Average Precision (mAP). *Precision* was defined as the proportion of correct detections relative to the total number of detections made, whereas *recall* represented the model's ability to identify the spores present in the images. The mAP metric was used to jointly assess classification and localization

performance. Specifically, mAP@0.5 considered detections with an intersection over union (IoU) value greater than 0.5 as correct, whereas mAP@0.5:0.95 corresponded to the average calculated across IoU thresholds from 0.5 to 0.95 in increments of 0.05 (Zhang et al. 2015; Ultralytics 2025).

In the context of aerobiological sampling, the main objective is to achieve accurate spore classification rather than exact localization within the image. For this reason, greater relevance was assigned to *recall* and *precision* when selecting the best model for each fungal genus, compared with metrics that more strictly penalize minor localization errors, such as mAP@0.5:0.95 (Kubera et al. 2022). Accordingly, among the trained models, priority was given to the one showing the highest mean *recall* on the validation set. When two models exhibited comparable *recall* values, *precision* and mAP@0.5 were used as tie-breaking criteria to ensure that the selected model, in addition to being sensitive to the presence of spores, retained a reasonable localization quality of the predicted bounding boxes.

2.5. Comparative analysis with other models

The comparison among the four models was conducted on the test subset, which consisted exclusively of real samples not used during training or validation. To ensure homogeneous evaluation conditions, all models were tested using a confidence threshold of 0.25 and an IoU threshold of 0.45 for non-maximum suppression. *Precision*, *recall*, F1-score, and mAP@0.5 were reported for the models overall, together with *recall* for each fungal genus. The selection of the optimal model followed the criteria defined in the previous section.

In addition to predictive performance, computational efficiency indicators relevant to the application of the system in aerobiological monitoring were considered, including the number of trainable parameters and the effective training epochs. Performance by fungal genus was also analyzed to identify differences among architectures and possible difficulties associated with genera showing morphological similarity. For the model with the best overall performance, the confusion matrix was examined in both absolute values and class-normalized form to interpret the main classification errors and guide possible improvements to the dataset.

2.6. Operational validation: automated vs. manual spore counting

To compare automated and manual quantification, an additional set of 516 images not used during training was selected. Each image was independently analyzed by trained personnel through microscopic observation and by the selected best-performing model. For both methods, the number of spores identified per genus was recorded, and the association between counts was evaluated using Spearman's correlation coefficient.

3. Results

3.1. Comparative analysis with other models

The overall comparison of the evaluated architectures showed superior performance of the YOLO26 family relative to the Faster R-CNN-based models (Table 4). YOLO26l achieved the highest values of *recall* (0.812), *precision* (0.823), mAP@0.5 (0.846), and F1-score (0.817), followed by YOLO26m, which also showed high performance *(recall* = 0.782, *precision* = 0.794, mAP@0.5 = 0.822, and F1 = 0.787). In contrast, ViT-B/16 + Faster R-CNN showed intermediate performance, with a marked decrease in *precision* (0.502) and F1-score (0.583), whereas AlexNet + Faster R-CNN yielded the lowest values across all evaluated metrics (*recall* = 0.548, *precision* = 0.377, mAP@0.5 = 0.527, and F1 = 0.447). These results demonstrate the greater ability of the YOLO26 variants to detect and classify fungal spores in microscopic images, with YOLO26l emerging as the best overall-performing model.

From the training perspective, the two variants of the YOLO26 family converged at very similar epochs (140 for YOLO26l and 141 for YOLO26m), indicating comparable convergence behavior between the two configurations. However, despite the nearly identical number of training epochs, YOLO26l consistently outperformed YOLO26m across all evaluated metrics, with gains of 0.030 in recall, 0.029 in precision, 0.024 in mAP@0.5, and 0.030 in F1-score. This result suggests that the increase in model capacity translated into a real performance improvement without requiring appreciably longer training in terms of epochs.

In contrast, the ViT-B/16 + Faster R-CNN and AlexNet + Faster R-CNN models completed training at epoch 100, but with substantially lower performance. ViT-B/16 + Faster R-CNN showed intermediate behavior, whereas AlexNet + Faster R-CNN yielded the lowest values across all metrics. Taken together, these results indicate that a shorter training duration, expressed in number of epochs, did not translate into a better performance-efficiency relationship. On the contrary, the YOLO26 variants, and particularly YOLO26l, provided the best balance between predictive quality and training stability for the task of multiclass fungal spore detection.

Table 4
Comparison of the overall performance of the evaluated architectures.

Model	Epoch stop train	Recall	Precision	mAP50	F1
Yolo26m	141	0,782	0,794	0,822	0,787
Yolo26l	**140**	**0,812**	**0,823**	**0,846**	**0,817**
ViT-B/16 + Faster R-CNN	100	0,695	0,502	0,606	0,583
AlexNet + Faster R-CNN	100	0,548	0,377	0,527	0,447

At the genus level, *recall* showed consistent differences among the evaluated approaches (Table 5). Overall, YOLO26l was the most robust model, maintaining the highest or near-highest values for most genera, with particularly good performance for *Curvularia, Didymella, Ganoderma, Nigrospora*, and *Xylaria*. YOLO26m followed a similar trend, although with lower sensitivity for several genera. The ViT + Faster R-CNN detector was competitive for some genera, such as *Nigrospora* and *Xylaria*, and matched YOLO26l for *Ganoderma*, although its performance decreased markedly for *Cladosporium*. In contrast, AlexNet + Faster R-CNN showed the lowest sensitivity overall, especially for the more challenging genera. Taken together, these results suggest that the YOLO models, particularly the higher-capacity YOLO26l variant, provide more consistent detection in fields containing multiple spores, whereas region proposal-based approaches such as Faster R-CNN tend to lose sensitivity for genera with greater morphological variability or lower contrast, such as *Cladosporium*.

Table 5
Recall by genus for the evaluated models.

Genus	Recall			
	Yolo26m	**Yolo26l**	**ViT-B/16 + Faster R-CNN**	**AlexNet + Faster R-CNN**
Cladosporium	0,382	0,429	0,100	0,021
Coprinus	0,767	0,800	0,790	0,620
Curvularia	0,827	0,914	0,646	0,563
Didymella	0,833	0,861	0,722	0,611
Ganoderma	0,837	0,862	0,862	0,638
Leptosphaeria	0,950	0,862	0,621	0,517
Nigrospora	0,857	0,905	0,929	0,786
Xylaria	0,871	0,871	0,887	0,629

The confusion matrix of the selected model showed a clear predominance of the main diagonal, indicating good discrimination ability among the evaluated fungal genera (Fig. 6). In the normalized matrix, the highest proportions of correct classification were observed for *Nigrospora* (0.95) and *Curvularia* (0.93), followed by *Leptosphaeria* (0.86), *Didymella* (0.84), *Coprinus* (0.81), *Xylaria* (0.80), and *Ganoderma* (0.79). In contrast, *Cladosporium* showed the lowest proportion of correct classifications (0.46), indicating that it was the most difficult class to detect and classify correctly.

Model errors were mainly associated with false negatives, that is, real spores classified as background, rather than with confusion among fungal genera. This pattern was particularly evident for *Cladosporium*, where 54% of the instances were not detected as spores, and to a lesser extent for *Ganoderma* (21%), *Xylaria* (20%), *Coprinus* (19%), and *Didymella* (16%). By contrast, direct confusion between genera was limited and of low magnitude, occurring mainly in isolated errors between *Leptosphaeria* and *Ganoderma*, and between *Nigrospora* and *Leptosphaeria* (≈ 0.03 in the normalized matrix). Overall, these results indicate that once a spore was detected, the model generally tended to assign the correct genus, and that the main source of error lay in missed detections (Fig. 6).

The absolute confusion matrix confirmed this behavior. In addition to the high concentration of correct predictions along the diagonal, the background class constituted the main source of residual error, both as the destination of false negatives and as the source of false positives. In particular, false detections in background regions were concentrated mainly in *Cladosporium* (33 cases), *Coprinus* (29 cases), and *Xylaria* (27 cases), whereas they were less frequent for the remaining genera. This pattern suggests that the main limitation of the model did not lie in separating morphologically similar genera, but rather in distinguishing spores from background structures with comparable visual appearance in some microscopic images (Fig. 6).

3.2. Operational validation: automated vs. manual spore counting

In the external test set, comprising 516 images and 1179 instances, YOLO26l achieved an overall precision of 0.803, a *recall* of 0.659, an mAP@0.5 of 0.748, and an mAP@0.5:0.95 of 0.649. These results indicate good classification capability on previously unseen images, although with reduced sensitivity relative to the internal evaluation. At the genus level, the best performance was observed for *Curvularia* (*precision* = 0.955, *recall* = 0.840, mAP@0.5 = 0.914), *Ganoderma* (0.906, 0.821, and 0.850), *Didymella* (0.832, 0.782, and 0.815), and *Coprinus* (0.797, 0.682, and 0.745). In contrast, *Cladosporium* showed the lowest performance, with a *recall* of 0.211 and an mAP@0.5 of 0.379, followed by *Xylaria*, which exhibited high precision (0.896) but lower detection capacity (*recall* = 0.518).

This behavior was consistent with the operational validation, in which the comparison between automated and manual counting showed positive and significant associations for all genera according to Spearman's correlation ($p < 0.001$) (Table 6). The coefficients ranged from 0.387 to 0.852, indicating associations of variable magnitude between the two methods. The highest values were recorded for *Curvularia, Didymella, Coprinus*, and *Ganoderma*, whereas *Cladosporium* showed the lowest correlation, confirming a less consistent model performance for this genus relative to the others.

Table 6
Spearman correlation between manual and automated counts for each genus.

Genus	*Cladosporium*	*Coprinus*	*Curvularia*	*Didymella*	*Ganoderma*	*Leptosphaeria*	*Nigrospora*	*Xylaria*
Spearman's ρ	0.387	0.782	0.852	0.824	0.778	0.721	0.652	0.683

From an operational perspective, manual counting of the 516 images required 2.8 h, equivalent to 19.5 s per image, whereas processing with the model required 1 min 39 s in total, that is, 0.19 s per image. This represents a substantial reduction in analysis time, with a processing speed approximately 102 times higher than that of manual counting. Overall, these results indicate that the model generalized unevenly across genera and that its main limitation in previously unseen samples was associated with missed spores, particularly in *Cladosporium*, rather than with the generation of false detections.

4. Discussion

The results obtained fall within the performance range previously reported for the detection of fungal spores and structures in microscopic images using deep learning. In studies combining RGB microscopic images with convolutional networks to identify *Alternaria, Fusarium*, and *Botrytis* spores, reported *precision* values ranged from 64.5% to 83.55% (Javidan et al. 2024). Likewise, other studies based on YOLO-type detectors applied to microscopic images have achieved high *precision, recall*, and mAP@0.5 values for fungal species detection, with metrics approaching 95% under controlled conditions (Zhao et al. 2024).

Although these studies demonstrate notable progress in spore detection from microscopic images, most have not been developed within the context of aerobiological sampling. In this field, encouraging results have been reported for the detection of *Alternaria* in air, with *precision* values close to 91% and *recall* around 94% using automated approaches (González-Alonso et al. 2023). In parallel, improvements have also been proposed for real-time automatic monitoring systems based on digital holography for the environmental detection of *Alternaria* (Espinosa et al. 2019). However, these applications have focused on one or only a few species, which remains limited given the high diversity of spores present in the atmosphere (O'Gorman and Fuller 2008; Pashley et al. 2012).

Consequently, the development of tools specifically oriented toward automatic multigenus classification and quantification in aerobiology remains incipient (Espinosa et al. 2019; González-Alonso et al. 2023). This gap is relevant because conventional aerobiological analysis examines only 10–12% of the microscope slide and estimates the daily spore concentration per cubic meter of air using a conversion factor (Galán et al. 2007). In addition to being time- and resource-intensive, this approach introduces uncertainty associated with human judgment; in pollen counting, an error close to 30% has been reported (Smith et al. 2019). For fungal spores, whose identification is usually more complex because of their high morphological variability, an equivalent estimate is not yet available. Therefore, achieving competitive performance relative to manual counting represents a relevant methodological and operational advance for aerobiological monitoring (Crespo-Michel et al. 2023).

Within this framework, the selected model (YOLO26l) showed adequate capacity to support the automatic quantification of spores in aerobiological sampling, although performance was uneven across genera. In previously unseen images, the best results were observed for *Curvularia, Ganoderma, Didymella*, and *Coprinus*, whereas *Cladosporium* represented the most challenging class. Figure 7 illustrates a representative example of the model output: in a micrograph containing multiple particles and background material, YOLO26l simultaneously identifies several spores by means of bounding boxes and assigns a genus together with a confidence level to each detection, thereby demonstrating its ability to localize and classify individual objects in complex visual fields. Even so, the comparison between automated and manual counting showed positive and significant associations for all genera ($p < 0.001$), indicating that, despite variations in sensitivity among genera, the model can be used as a tool for the identification and quantification of fungal spores in aerobiological studies.

The practical contribution of this approach lies in substantially reducing the operational bottleneck associated with conventional aerobiological analysis. In the Hirst-type volumetric method, microscopic processing and manual counting constitute the most demanding stage. A single preparation may require several hours of specialized work, particularly during episodes of high concentrations, which delays data availability. As a result, delays of between 1 and 9 days have been reported between counting, validation, and publication of results (Kubera et al. 2022; Tummon et al. 2024). In this context, implementing the model made it possible to automate the localization and counting of spores in 516 images, reducing total analysis time from 2.8 h by manual counting to 1 min 39 s with the automated system. This corresponds to a reduction from 19.5 s to 0.19 s per image and to a processing speed approximately 102 times higher. Such an operational gain favors the routine and more timely generation of daily data, with potential application in early warning systems and in supporting decision-making for sensitive populations exposed to bioaerosols (Tummon et al. 2024).

These operational benefits, however, depend on maintaining robust performance in the most prevalent and environmentally relevant genera. In this regard, *Cladosporium* sp. showed lower performance, with low *precision* and *recall* values. This behavior is consistent with previous reports in which *precision* for this genus decreases markedly relative to morphologically similar taxa, reaching ranges between 62% and 81% in systems based on holography and fluorescence (Bruffaerts et al. 2025). These limitations probably reflect the high intrageneric morphological variability and the difficulty of differentiating this taxon under real microscopic capture conditions. Future research should therefore evaluate specific strategies to improve its recognition, including augmentation targeted to aggregated morphologies, higher-capacity architectures, or the incorporation of preprocessing stages based on classical computer vision in order to reduce false positives and improve discrimination among genera.

Taken together, the results show that deep learning-based automation can contribute substantially to strengthening aerobiological monitoring, particularly by improving the timeliness and reproducibility of data. From an environmental

perspective, this broadens the possibilities for routine bioaerosol surveillance and for generating useful information to support risk management in exposed populations.

5. Conclusion

This study provides evidence that deep learning-based automatic detection models can be effectively integrated into aerobiological sampling, not merely as a microscopy classification exercise, but as a tool aimed at the operational quantification of airborne fungal spores. Its main novelty lies in the implementation and validation of a multigenus framework for eight relevant taxa, evaluated under conditions inherent to aerobiological analysis and benchmarked against traditional manual counting. Among the compared architectures, YOLO26l showed the best general performance and the greatest capability for multiclass detection in visual fields containing multiple particles.

Although performance was heterogeneous across genera—with stronger results for *Curvularia, Ganoderma, Didymella*, and *Coprinus*, and greater difficulties for *Cladosporium*—the agreement between automated and manual counting showed positive and significant associations for all genera, indicating that the system consistently reproduced the general abundance patterns observed by microscopy.

From an applied perspective, the proposed approach reduces the time required for sample processing and enables the generation of more timely data, with potential implications for environmental bioaerosol surveillance, exposure tracking, and support for early warning systems and health risk assessment. Taken together, these findings position deep learning-based detection as a relevant contribution to strengthening and scaling aerobiological studies beyond approaches focused on one or only a few species.

Declarations

Competing Interests

The authors have no relevant financial or non-financial interests to disclose.

Ethical Approval

This is not applicable

Consent to Participate

This is not applicable

Consent to Publish

This is not applicable

Funding

This study was supported by the Department of Science, Technology and Innovation–COLCIENCIAS (Colombia) through the *Becas de Excelencia Doctoral del Bicentenario* program, which awarded a doctoral fellowship to Dámaris A. Jiménez-Uribe.

Author Contributions

All authors contributed to the conception and design of the study. The original idea of the article was developed by Dámaris A. Jiménez-Uribe and Alberto Patiño-Vanegas. Data collection was performed by Dámaris A. Jiménez-Uribe. Data curation and

formal analysis were carried out by Dámaris A. Jiménez-Uribe, Jeison D. Jimenez, and Deyson Gómez Sánchez. The first draft of the manuscript was written by Alberto Patiño-Vanegas, Dámaris A. Jiménez-Uribe, and Deyson Gómez Sánchez. Carolina Rubiano-Labrador, Hernando Altamar-Mercado, and Rosa Acevedo-Barrios reviewed and edited previous versions of the manuscript. All authors read and approved the final manuscript.

Acknowledgments

The authors would like to acknowledge the support provided by the master's degree scholarship program in engineering at the Universidad Tecnologica de Bolivar (UTB) in Cartagena, Colombia.

Data availability

The datasets generated and analyzed during the current study, including the annotated image dataset and the data supporting the reported results, are available from the corresponding author on reasonable request.

References

1. Adamov S, Lemonis N, Clot B, Crouzy B, Gehrig R, Graber M-J, Sallin C, Tummon F (2024) On the measurement uncertainty of Hirst-type volumetric pollen and spore samplers. Aerobiologia 40(1):77–91. https://doi.org/10.1007/s10453-021-09724-5
2. Astolfi G, Gonçalves AB, Menezes GV, Borges FSB, Astolfi ACMN, Matsubara ET, Alvarez M, Pistori H (2020) POLLEN73S: an image dataset for pollen grains classification. Ecol Inf 60:101165. https://doi.org/10.1016/j.ecoinf.2020.101165
3. Battiato S, Ortis A, Trenta F, Ascari L, Politi M, Siniscalco C (2020) POLLEN13K: a large scale microscope pollen grain image dataset. In: 2020 IEEE International Conference on Image Processing (ICIP). IEEE, pp 2456–2460. https://doi.org/10.1109/ICIP40778.2020.9190776
4. Bi J, Li K, Zheng X, Zhang G, Lei T (2025) SPDC-YOLO: an efficient small target detection network based on improved YOLOv8 for drone aerial image. Remote Sens 17(4):685. https://doi.org/10.3390/rs17040685
5. Blais-Lecours P, Perrott P, Duchaine C (2015) Non-culturable bioaerosols in indoor settings: impact on health and molecular approaches for detection. Atmos Environ 110:45–53. https://doi.org/10.1016/j.atmosenv.2015.03.039
6. Bochkovskiy A, Wang C-Y, Liao H-YM (2020) YOLOv4: optimal speed and accuracy of object detection. https://doi.org/10.48550/arXiv.2004.10934. arXiv:2004.10934
7. Bruffaerts N, Graf E, Matavulj P, Tiwari A, Pyrri I, Zeder Y, Erb S, Plaza M, Dietler S, Bendinelli T, D'hooge E, Sikoparija B (2025) Advancing automated identification of airborne fungal spores: guidelines for cultivation and reference dataset creation. Aerobiologia 41(2):505–525. https://doi.org/10.1007/s10453-025-09864-y
8. Buslaev A, Iglovikov VI, Khvedchenya E, Parinov A, Druzhinin M, Kalinin AA (2020) Albumentations: fast and flexible image augmentations. Information 11(2):125. https://doi.org/10.3390/info11020125
9. Cao C, Jiang W, Wang B, Fang J, Lang J, Tian G, Jiang J, Zhu TF (2014) Inhalable microorganisms in Beijing's PM2.5 and PM10 pollutants during a severe smog event. Environ Sci Technol 48(3):1499–1507. https://doi.org/10.1021/es4048472
10. Cao N, Meyer M, Thiele L, Saukh O (2020) Pollen video library for benchmarking detection, classification, tracking and novelty detection tasks: dataset. In: Proceedings of the Third Workshop on Data: Acquisition to Analysis. Association for Computing Machinery, New York, NY, USA, pp 23–25. https://doi.org/10.1145/3419016.3431487
11. Casado-García A, del-Canto A, Sanz-Saez A, Pérez-López U, Bilbao-Kareaga A, Fritschi FB, Miranda-Apodaca J, Muñoz-Rueda A, Sillero-Martínez A, Yoldi-Achalandabaso A, Lacuesta M, Heras J (2020) LabelStoma: a tool for stomata detection based on the YOLO algorithm. Comput Electron Agric 178:105751. https://doi.org/10.1016/j.compag.2020.105751
12. Charalampopoulos A, Damialis A, Vokou D (2022) Spatiotemporal assessment of aeromycoflora under differing urban green space, sampling height, and meteorological regimes: the atmospheric fungiscape of Thessaloniki, Greece. Int J Biometeorol 66(5):895–909. https://doi.org/10.1007/s00484-022-02247-9

13. Crespo-Michel A, Alonso-Arévalo MA, Hernández-Martínez R (2023) Developing a microscope image dataset for fungal spore classification in grapevine using deep learning. J Agric Food Res 14:100805. https://doi.org/10.1016/j.jafr.2023.100805
14. Dosovitskiy A, Beyer L, Kolesnikov A, Weissenborn D, Zhai X, Unterthiner T, Dehghani M, Minderer M, Heigold G, Gelly S, Uszkoreit J, Houlsby N (2021) An image is worth 16x16 words: transformers for image recognition at scale. In: International Conference on Learning Representations (ICLR). https://doi.org/10.48550/arXiv.2010.11929
15. Dwyer B, Nelson J, Hansen T (2026) Roboflow (Version 1.0) [Software]. Available from: https://roboflow.com. Accessed 1 June 2026
16. Egan C, Li D-W, Klironomos J (2014) Detection of arbuscular mycorrhizal fungal spores in the air across different biomes and ecoregions. Fungal Ecol 12:26–31. https://doi.org/10.1016/j.funeco.2014.06.004
17. Espinosa KCS, Chávez MA, Ramírez IP, Flores TIR, Rodríguez MJA (2019) Fungal diversity in the atmosphere of Havana (Cuba) during three low-rainfall periods (in Spanish). Rev Int Contam Ambient 35(1):137–150. https://doi.org/10.20937/RICA.2019.35.01.10
18. France I, Duller AWG, Duller GAT, Lamb HF (2000) A new approach to automated pollen analysis. Quat Sci Rev 19(6):537–546. https://doi.org/10.1016/S0277-3791(99)00021-9
19. Galán C, Cariñanos P, Alcázar P, Domínguez E (2007) Quality and management manual of the Spanish Aerobiology Network (in Spanish). Servicio de Publicaciones de la Universidad de Córdoba, Córdoba
20. Gheorghe C, Duguleana M, Boboc R, Postelnicu C (2024) Analyzing real-time object detection with YOLO algorithm in automotive applications: a review. Comput Model Eng Sci 141(3):1939–1981. https://doi.org/10.32604/cmes.2024.054735
21. González-Alonso M, Boldeanu M, Koritnik T, Gonçalves J, Belzner L, Stemmler T, Gebauer R, Grewling Ł, Tummon F, Maya-Manzano JM, Ariño AH, Schmidt-Weber C, Buters J (2023) Alternaria spore exposure in Bavaria, Germany, measured using artificial intelligence algorithms in a network of BAA500 automatic pollen monitors. Sci Total Environ 861:160180. https://doi.org/10.1016/j.scitotenv.2022.160180
22. Grinn-Gofroń A, Bosiacka B (2015) Effects of meteorological factors on the composition of selected fungal spores in the air. Aerobiologia 31(1):63–72. https://doi.org/10.1007/s10453-014-9347-1
23. Hidayatullah P, Tubagus R (2026) YOLO26: a comprehensive architecture overview and key improvements. https://doi.org/10.48550/arXiv.2602.14582. arXiv:2602.14582
24. Humbal C, Gautam S, Trivedi U (2018) A review on recent progress in observations, and health effects of bioaerosols. Environ Int 118:189–193. https://doi.org/10.1016/j.envint.2018.05.053
25. Javidan SM, Banakar A, Vakilian KA, Ampatzidis Y, Rahnama K (2024) Diagnosing the spores of tomato fungal diseases using microscopic image processing and machine learning. Multimed Tools Appl 83(26):67283–67301. https://doi.org/10.1007/s11042-024-18214-y
26. Jiménez-Uribe DA, Acevedo-Barrios R, Rubiano-Labrador C, Cariñanos P (2026) Relationship of airborne fungal spores to epidemiological data on respiratory disease: a systematic review. Aerobiologia 42(1):11. https://doi.org/10.1007/s10453-025-09890-w
27. Krizhevsky A, Sutskever I, Hinton GE (2017) ImageNet classification with deep convolutional neural networks. Commun ACM 60(6):84–90. https://doi.org/10.1145/3065386
28. Kubera E, Kubik-Komar A, Kurasiński P, Piotrowska-Weryszko K, Skrzypiec M (2022) Detection and recognition of pollen grains in multilabel microscopic images. Sensors 22(7):2690. https://doi.org/10.3390/s22072690
29. Lee BU, Lee G, Heo KJ (2016) Concentration of culturable bioaerosols during winter. J Aerosol Sci 94:1–8. https://doi.org/10.1016/j.jaerosci.2015.12.002
30. Levetin E, Horner WE, Scott JA (2016) Taxonomy of allergenic fungi. J Allergy Clin Immunol Pract 4(3):375–385. .e1 https://doi.org/10.1016/j.jaip.2015.10.012
31. Li P, Flenley JR (1999) Pollen texture identification using neural networks. Grana 38(1):59–64. https://doi.org/10.1080/001731300750044717

32. Lundbäck B, Backman H, Lötvall J, Rönmark E (2016) Is asthma prevalence still increasing? Expert Rev Respir Med 10(1):39–51. https://doi.org/10.1586/17476348.2016.1114417
33. Marcos JV, Nava R, Cristóbal G, Redondo R, Escalante-Ramírez B, Bueno G, Déniz Ó, González-Porto A, Pardo C, Chung F, Rodríguez T (2015) Automated pollen identification using microscopic imaging and texture analysis. Micron 68:36–46. https://doi.org/10.1016/j.micron.2014.09.002
34. Nair A, Manomohan NK, Reddy H, Pandey S, Kadam P (2021) Fungus detection and identification using computer vision techniques and convolution neural networks. In: 2021 International Conference on Smart Generation Computing, Communication and Networking (SMART GENCON). IEEE, pp 1–6. https://doi.org/10.1109/SMARTGENCON51891.2021.9645827
35. Nieguitsila A, Deville M, Jamal T, Halos L, Berthelemy M, Chermette R, Latouche S, Arné P, Guillot J (2007) Evaluation of fungal aerosols using Temporal Temperature Gradient Electrophoresis (TTGE) and comparison with culture. J Microbiol Methods 70(1):86–95. https://doi.org/10.1016/j.mimet.2007.03.021
36. O'Gorman CM, Fuller HT (2008) Prevalence of culturable airborne spores of selected allergenic and pathogenic fungi in outdoor air. Atmos Environ 42(18):4355–4368. https://doi.org/10.1016/j.atmosenv.2008.01.009
37. Pashley CH, Fairs A, Free RC, Wardlaw AJ (2012) DNA analysis of outdoor air reveals a high degree of fungal diversity, temporal variability, and genera not seen by spore morphology. Fungal Biol 116(2):214–224. https://doi.org/10.1016/j.funbio.2011.11.004
38. Pomés A, Chapman MD, Wünschmann S (2016) Indoor allergens and allergic respiratory disease. Curr Allergy Asthma Rep 16(6):43. https://doi.org/10.1007/s11882-016-0622-9
39. Ren S, He K, Girshick R, Sun J (2017) Faster R-CNN: towards real-time object detection with region proposal networks. IEEE Trans Pattern Anal Mach Intell 39(6):1137–1149. https://doi.org/10.1109/TPAMI.2016.2577031
40. Sapkota R, Flores-Calero M, Qureshi R, Badgujar C, Nepal U, Poulose A, Zeno P, Vaddevolu UBP, Khan S, Shoman M, Yan H, Karkee M (2025) YOLO advances to its genesis: a decadal and comprehensive review of the You Only Look Once (YOLO) series. Artif Intell Rev 58(9):274. https://doi.org/10.1007/s10462-025-11253-3
41. Smith M, Oteros J, Schmidt-Weber C, Buters JTM (2019) An abbreviated method for the quality control of pollen counters. Grana 58(3):185–190. https://doi.org/10.1080/00173134.2019.1570327
42. Soltani Nezhad F, Rahnama K, Javidan SM, Asefpour Vakilian K (2024) Application of microscopic image processing and artificial intelligence detecting and classifying the spores of three novel species of Trichoderma. Discov Appl Sci 6(12):669. https://doi.org/10.1007/s42452-024-06388-x
43. Spicer RC, Gangloff HJ (2010) Differences in detection frequency as a bioaerosol data criterion for evaluating suspect fungal contamination. Build Environ 45(5):1304–1311. https://doi.org/10.1016/j.buildenv.2009.11.012
44. Tahir MW, Zaidi NA, Rao AA, Blank R, Vellekoop MJ, Lang W (2018) A fungus spores dataset and a convolutional neural network based approach for fungus detection. IEEE Trans Nanobiosci 17(3):281–290. https://doi.org/10.1109/TNB.2018.2839585
45. Tello-Mijares S, Flores F (2016) A novel method for the separation of overlapping pollen species for automated detection and classification. Comput Math Methods Med 2016:5689346. https://doi.org/10.1155/2016/5689346
46. Tummon F, Adams-Groom B, Antunes CM, Bruffaerts N, Buters J, Cariñanos P, Celenk S, Choël M, Clot B, Cristofori A, Crouzy B, Damialis A, Fernández AR, González DF, Galán C, Gedda B, Gehrig R, Gonzalez-Alonso M, Gottardini E, Gros-Daillon J, Hajkova L, O'Connor D, Östensson P, Oteros J, Pauling A, Pérez-Badia R, Rodinkova V, Rodríguez-Rajo FJ, Ribeiro H, Sauliene I, Sikoparija B, Skjøth CA, Spanu A, Sofiev M, Sozinova O, Srnec L, Visez N, de Weger LA (2024) The role of automatic pollen and fungal spore monitoring across major end-user domains. Aerobiologia 40(1):57–75. https://doi.org/10.1007/s10453-024-09820-2
47. Twaroch T, Curin M, Sterflinger K, Focke-Tejkl M, Swoboda I, Valenta R (2016) Specific antibodies for the detection of Alternaria allergens and the identification of cross-reactive antigens in other fungi. Int Arch Allergy Immunol 170(4):269–278. https://doi.org/10.1159/000449415

48. Ultralytics (2025) YOLO performance metrics. Ultralytics Docs. https://docs.ultralytics.com/guides/yolo-performance-metrics. Accessed 15 July 2025
49. Waithe D, Brown JM, Reglinski K, Diez-Sevilla I, Roberts D, Eggeling C (2020) Object detection networks and augmented reality for cellular detection in fluorescence microscopy. J Cell Biol 219(10):e201903166. https://doi.org/10.1083/jcb.201903166
50. Zhang H, Cisse M, Dauphin YN, Lopez-Paz D (2018) Mixup: beyond empirical risk minimization. In: International Conference on Learning Representations (ICLR). https://doi.org/10.48550/arXiv.1710.09412
51. Zhang X, Feng X, Xiao P, He G, Zhu L (2015) Segmentation quality evaluation using region-based precision and recall measures for remote sensing images. ISPRS J Photogramm Remote Sens 102:73–84. https://doi.org/10.1016/j.isprsjprs.2015.01.009
52. Zhao E, Zhao H, Liu G, Jiang J, Zhang F, Zhang J, Luo C, Chen B, Yang X (2024) Automated recognition of conidia of nematode-trapping fungi based on improved YOLOv8. IEEE Access 12:81314–81328. https://doi.org/10.1109/ACCESS.2024.3407853
53. Zolfaghari M, Sajedi H (2024) Automated classification of pollen grains microscopic images using cognitive attention based on human two visual streams hypothesis. PLoS ONE 19(11):e0309674. https://doi.org/10.1371/journal.pone.0309674

Figures

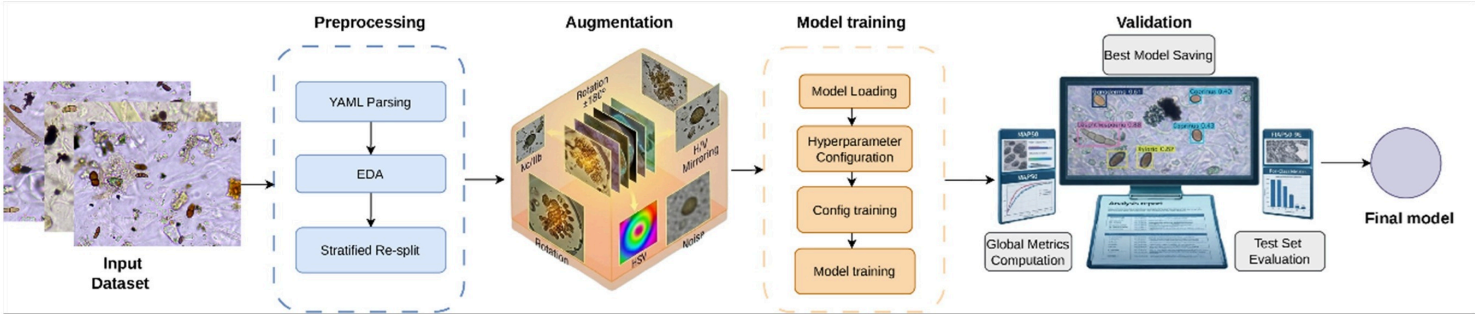


Figure 1

System Pipeline

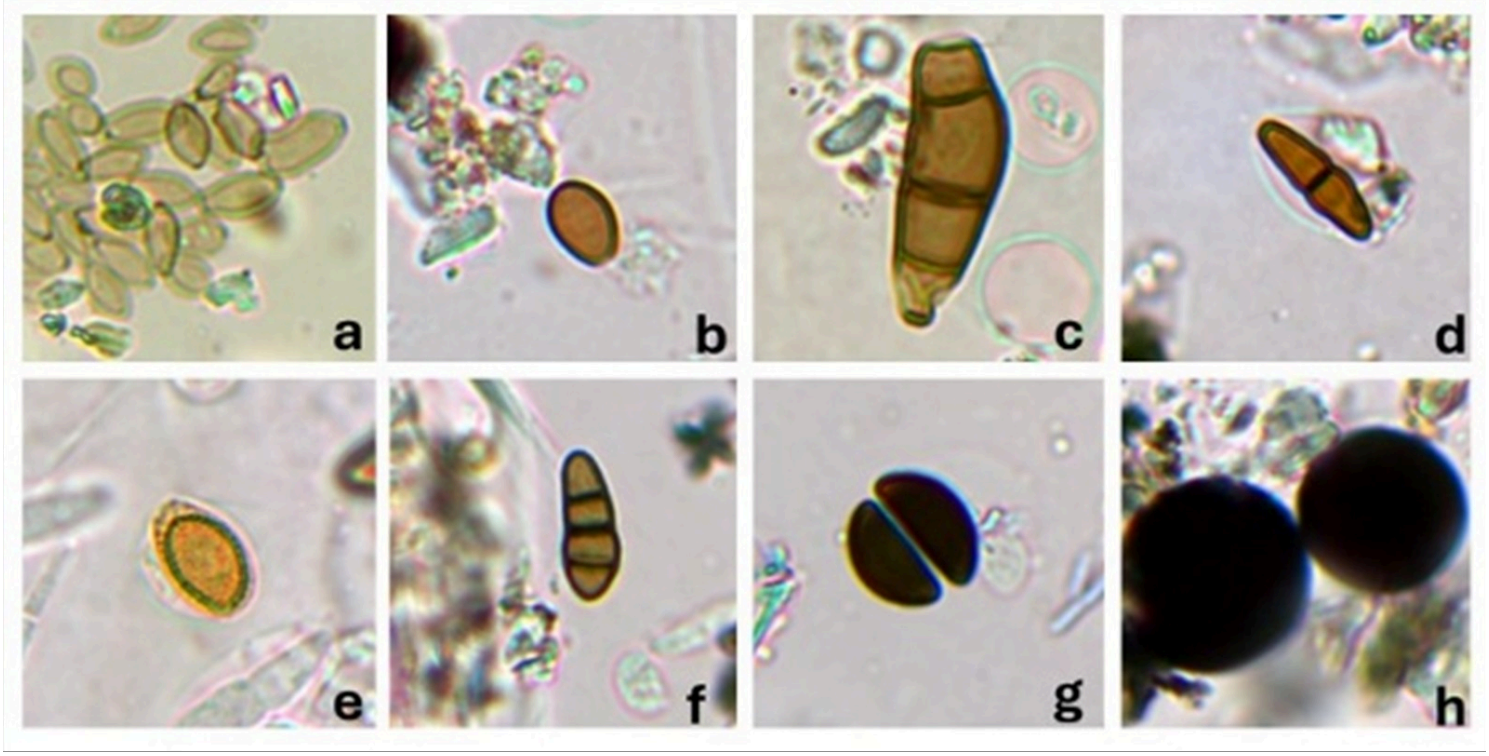


Figure 2

Types of fungal spores selected for the study. **a**. Cladosporium sp. **b**. Coprinus sp. **c.** Curvularia sp. **d.** Didymella sp. **e.** Ganoderma sp. **f.** Leptosphaeria sp. **g.** Xylaria sp. **h.** Nigrospora sp.

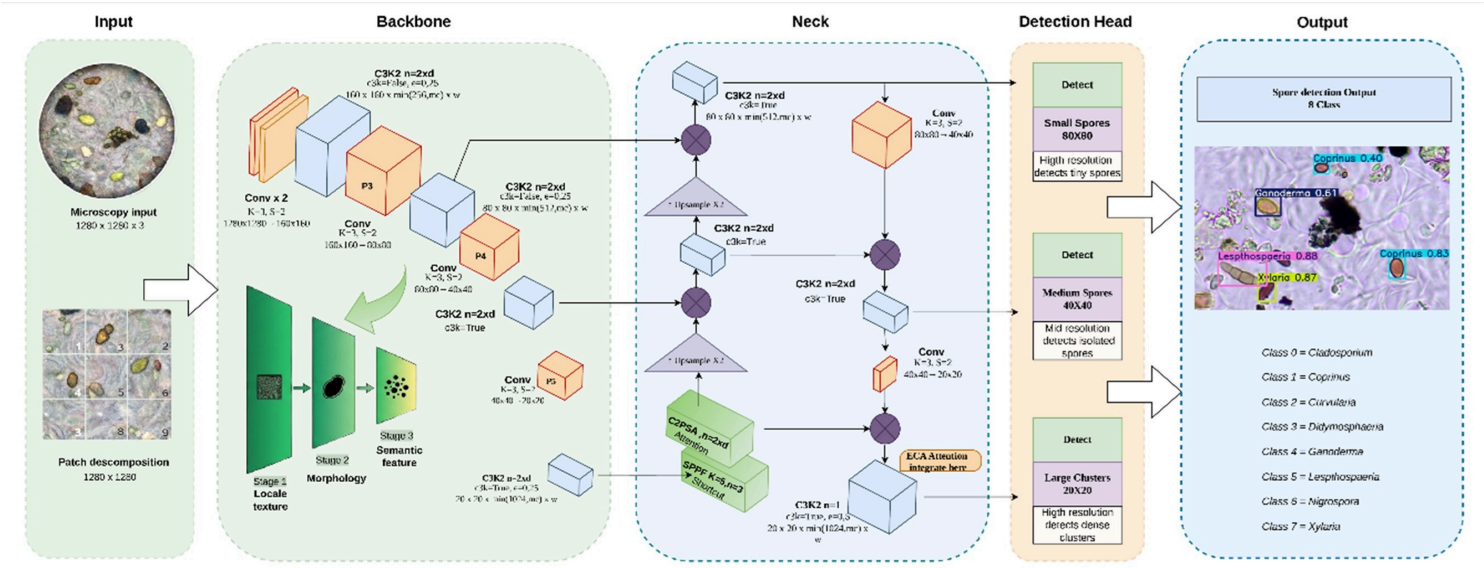


Figure 3

YOLO26 architecture for detection and classification of airborne fungal spores (8 class)

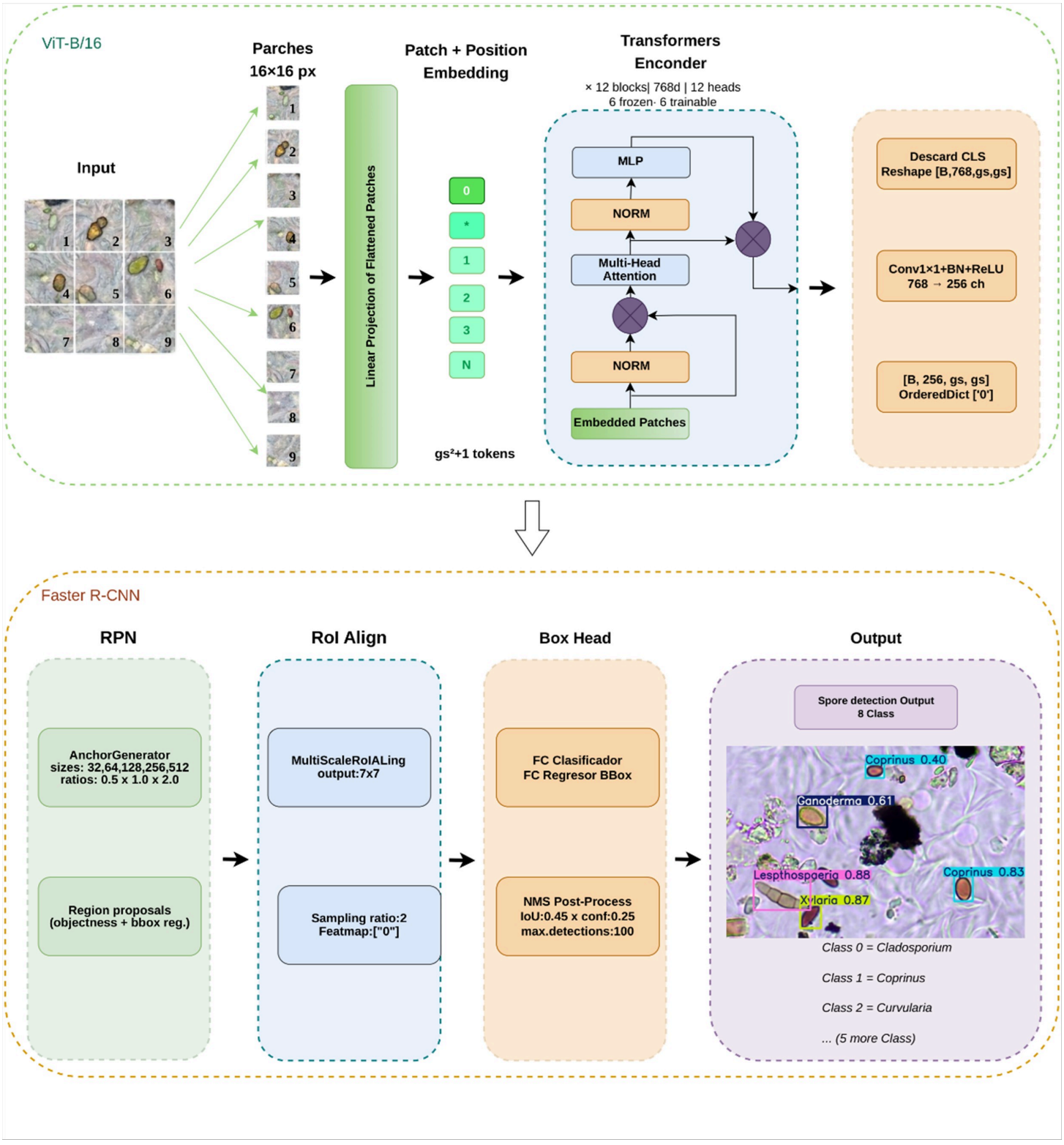


Figure 4

ViT-B/16 + Faster R-CNN architecture for detection and classification of airborne fungal spores (8 class).

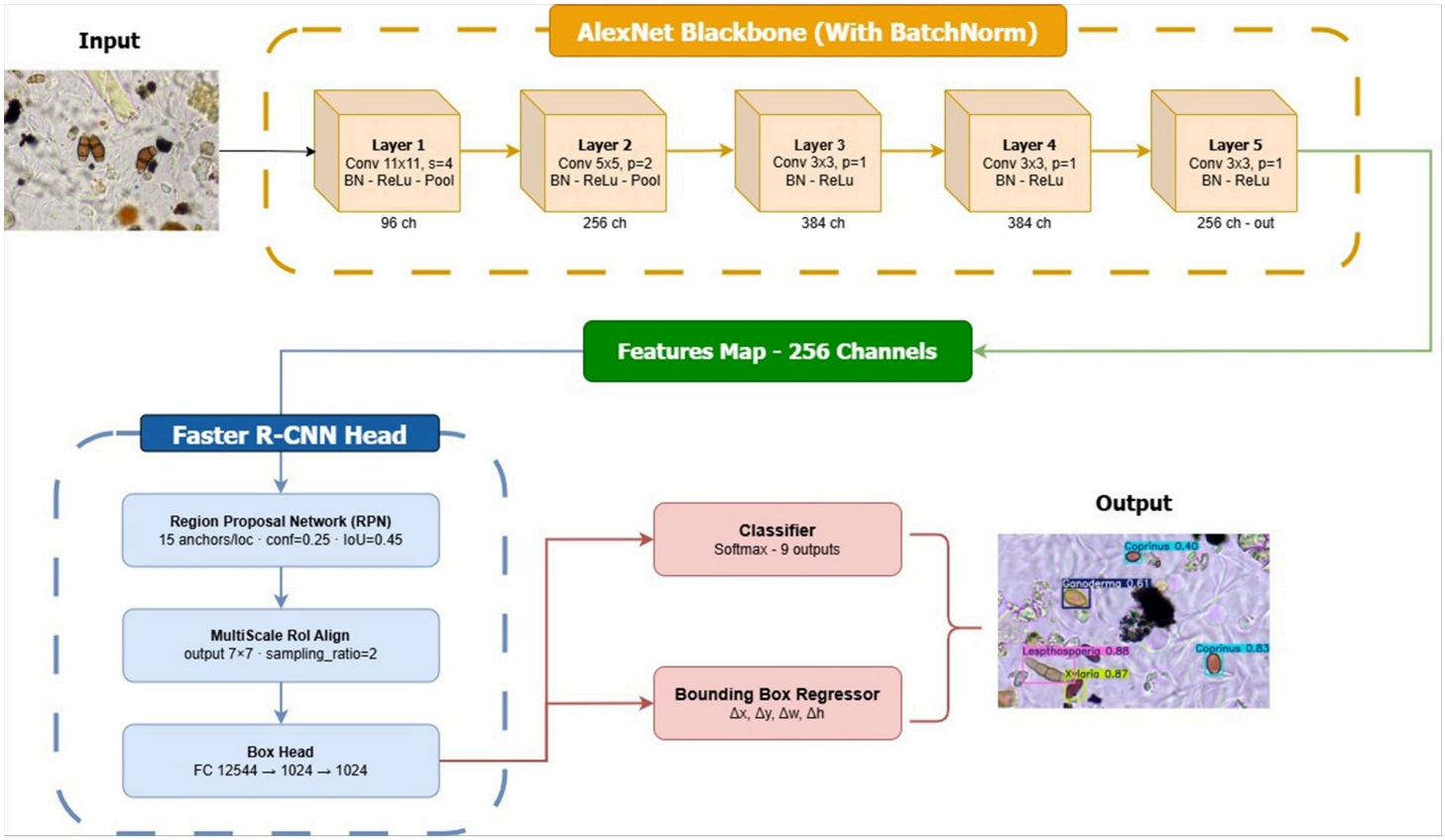


Figure 5

AlexNEt architecture for detection and classification of airborne fungal spores (8 class).

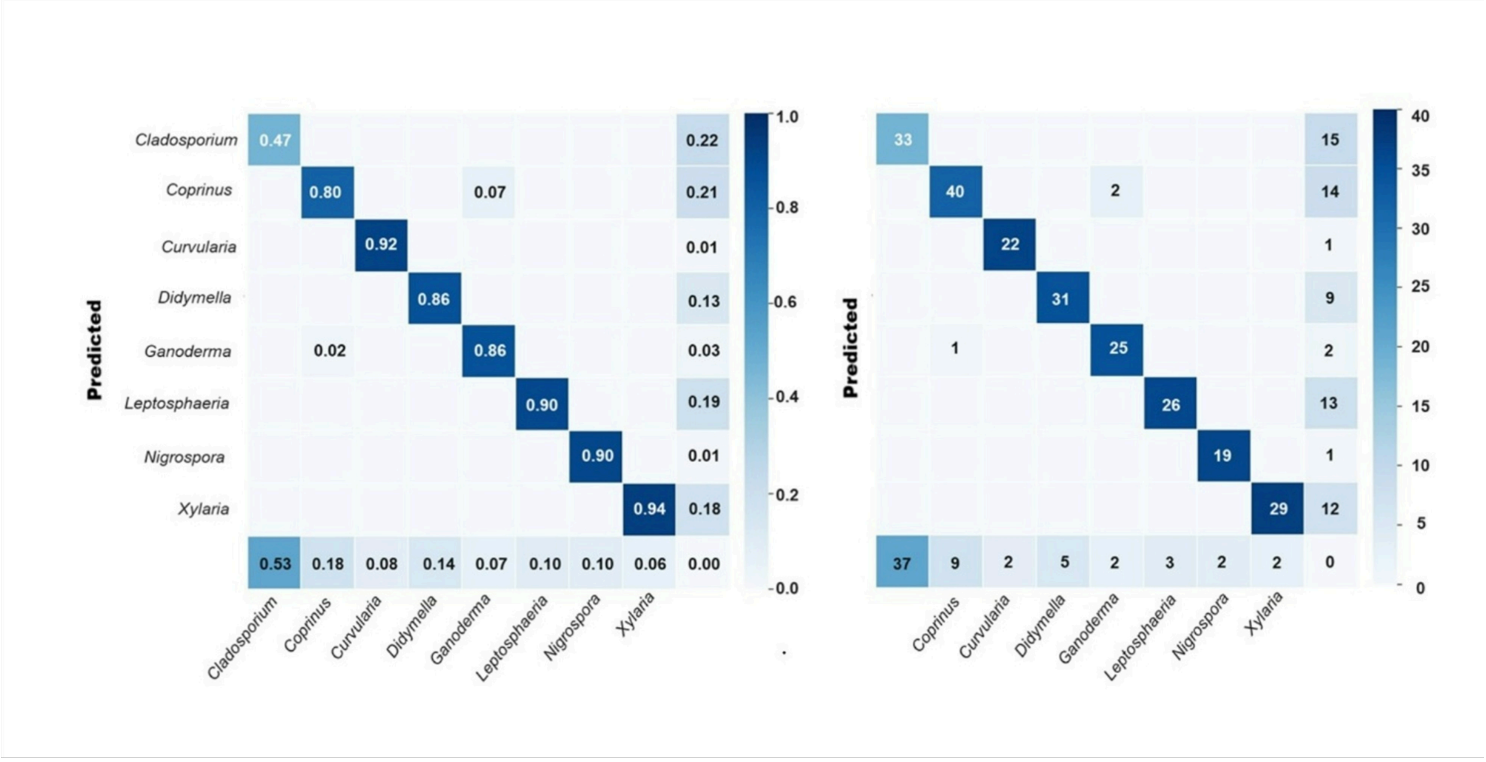


Figure 6

Absolute and normalized confusion matrices of the YOLO26l model on the test set

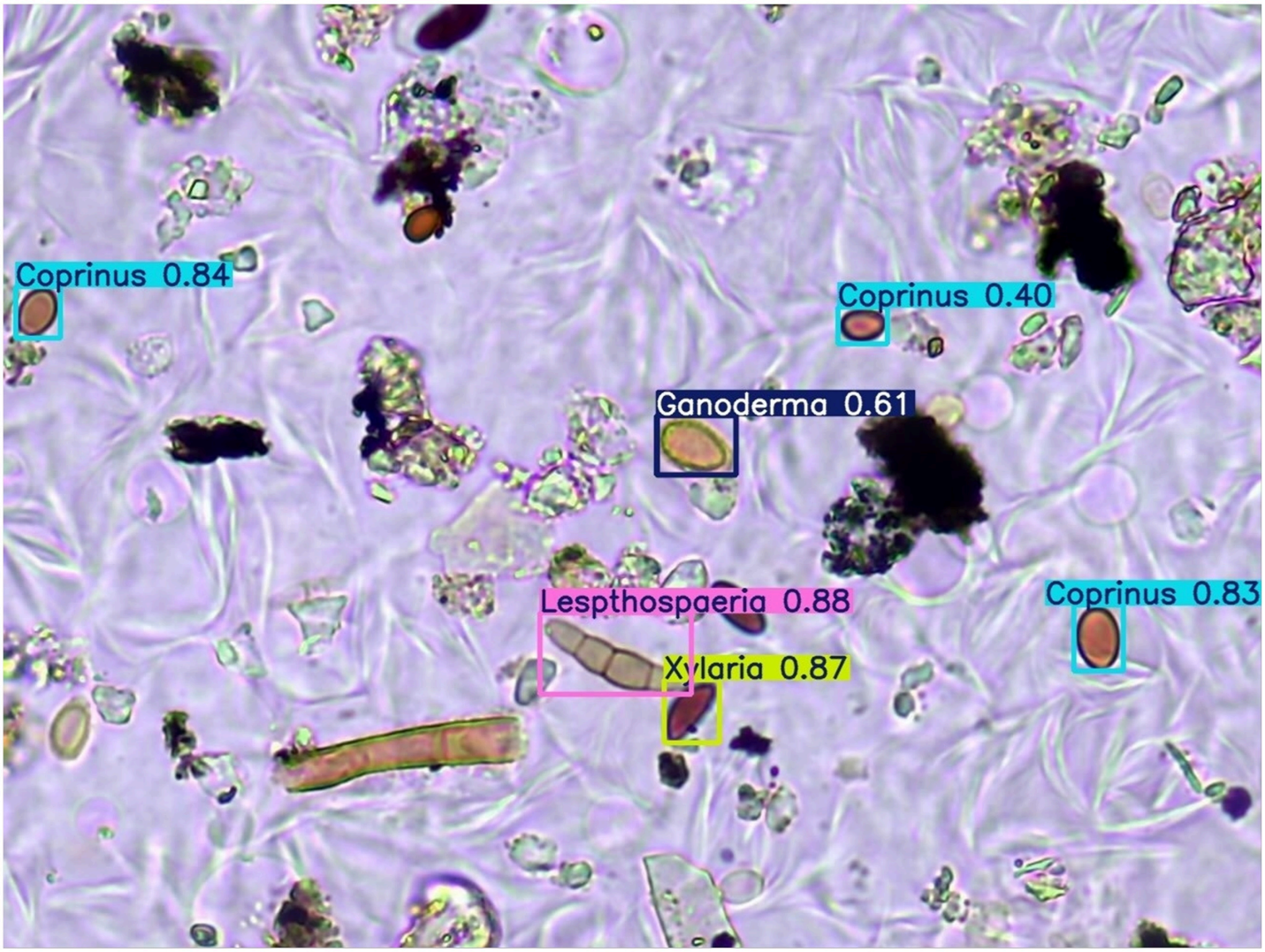


Figure 7

Example of model output on an augmented processed image